Journal of Sound and Vibration (1992) **155**(2), 209–230

SPECTRAL COUPLING ISSUES IN A TWO-DEGREE-OF-FREEDOM SYSTEM WITH CLEARANCE NON-LINEARITIES

C. PADMANABHAN AND R. SINGH

Department of Mechanical Engineering, The Ohio State University, Columbus, Ohio 43210-1107, *U.S.A.*

(*Received* 24 *April* 1990 *and in final form* 16 *January* 1991)

In an earlier study [14], the frequency response characteristics of a multi-degree-of-freedom system with clearance non-linearities were presented. The current study is an extension of this prior work and deals specifically with the issue of dynamic interactions between resonances. The harmonic balance method, digital solutions and analog computer simulation are used to investigate a two-degree-of-freedom system under a mean load, when subjected to sinusoidal excitations. The existence of harmonic, periodic and chaotic solutions is demonstrated using digital simulation. The method of harmonic balance is employed to construct approximate solutions at the excitation frequency which are then used to classify weak, moderate and strong non-linear spectral interactions. The effects of parameters such as damping ratio, mean load, alternating load and frequency spacing between the resonances have been quantified. The applicability of the methodology is demonstrated through the following practical examples: (i) neutral gear rattle in an automotive transmission system; and (ii) steady state characteristics of a spur gear pair with backlash. In the second case, measured dynamic transmission error data at the gear mesh frequency are used to investigate spectral interactions. Limitations associated with solution methods and interaction classification schemes are also discussed.

1. INTRODUCTION

Many mechanical systems exhibit non-linearities which are often non-analytical and non-differentiable. One typical example is the clearance non-linearity which can be used to describe the backlash in a gear pair, preset or preload in springs and a bilinear dry friction clutch. A number of investigators [1–15] have analyzed such non-linearities using various methods, including piecewise linear techniques [1–6], digital simulation [1, 2, 6–10], analog simulation [8, 11] and the method of harmonic balance [12–15]. Most of these analyses have emphasized the determination of the actual time domain response for a harmonic excitation and these have been essentially limited to a single-degree-of-freedom (SDOF) system. A detailed literature review of SDOF analyses can be found in a recent paper [12].

Multi-degree-of-freedom (MDOF) systems with clearances have been studied by only a few investigators [6, 7, 9, 10, 14, 15]. For instance, Singh *et al.* [10] investigated a four-degree-of-freedom non-linear model to study automotive transmission neutral rattle problems. However, they did not address the issue of spectral interactions or coupling of resonances. Comparin and Singh [14] have discussed it qualitatively. Furthermore, while analyzing coupled impact pairs they have assumed that the resonances in a MDOF system are weakly coupled, which essentially reduces the formulation to several uncoupled SDOF systems. Haddow *et al.* [16] examined the issue of coupling in a two-degree-of-freedom system with quadratic non-linearities. However, previous studies [12–15] have shown that

0022–460X/92/110209+22 $03.00/0

the dynamic behavior of a system with continuous non-linearities is quite different from a system with discontinuous non-linearities.

Based on the literature review, it is clear that there is a definite need for an analytical study of the spectral interactions in a MDOF system with clearance non-linearities. This is the main focus of the paper, but unlike reference [16], combination or internal resonances are not considered here. The present study, an extension to reference [14], employs a two-degree-of-freedom model to illustrate key issues.

2. PROBLEM FORMULATION

The equations of motion of a three-degree-of-freedom semi-definite system, as shown in Figure 1, for sinusoidal excitation at frequency $\bar{\Omega}$ but under mean loads $\bar{F}_{1m}$ and $\bar{F}_{2m}$ are as follows in terms of $\bar{q}_1$ and $\bar{q}_2$:

$$[M]\{\ddot{\bar{q}}(t)\}+[C]\{\dot{\bar{q}}(t)\}+[K]\{f(\bar{q}(t))\}=\{F(t)\}, \tag{1}$$

$$[M]=\begin{bmatrix} m_{q1} & 0 \\ 0 & m_{q2} \end{bmatrix}, \qquad m_{q1}=\frac{m_1 m_2}{m_1+m_2}, \qquad m=\frac{m_2 m_3}{m_2+m_3}, \tag{2-4}$$

$$[C]=\begin{bmatrix} c_1 & -\dfrac{m_{q1}c_2}{m_2} \\ -\dfrac{m_{q2}c_1}{m_2} & c_2 \end{bmatrix}, \qquad [K]=\begin{bmatrix} k_1 & -\dfrac{k_2 m_{q1}}{m_2} \\ -\dfrac{k_1 m_{q2}}{m_2} & k_2 \end{bmatrix}, \tag{5, 6}$$

$$\{\bar{q}(t)\}=\begin{Bmatrix} \bar{q}_1(t) \\ \bar{q}_2(t) \end{Bmatrix}, \qquad \{f(\bar{q})\}=\begin{Bmatrix} f_1(\bar{q}_1) \\ f_2(\bar{q}_2) \end{Bmatrix}, \qquad \{F\}=\begin{Bmatrix} \bar{F}_{1m}+\bar{F}_{1a}\sin(\bar{\Omega}t) \\ \bar{F}_{2m} \end{Bmatrix}, \tag{7-9}$$

$$\bar{F}_{1m}+\bar{F}_{1a}\sin(\bar{\Omega}t)=\frac{m_{q1}}{m_1}F_1-\frac{m_{q1}}{m_2}F_2, \qquad \bar{F}_{2m}=\frac{m_{q2}}{m_2}F_2-\frac{m_{q2}}{m_3}F_3, \tag{10, 11}$$

where $f_1(\bar{q}_1)$ and $f_2(\bar{q}_2)$ describe the non-linear stiffness elements. A dimensionless form of equation (1) can be obtained by using $q_i=\bar{q}_i/b_c$, $\omega_n=\sqrt{k_1/m_{q1}}$ and $\tau=\omega_n t$, where b_c is the characteristic length. Furthermore, define a non-dimensional excitation frequency $\Omega=\bar{\Omega}/\omega_n$ to yield the following governing equations in dimensionless form:

$$[I]\begin{Bmatrix} \ddot{q}_1 \\ \ddot{q}_2 \end{Bmatrix}+[\Xi]\begin{Bmatrix} \dot{q}_1 \\ \dot{q}_2 \end{Bmatrix}+[\Psi]\begin{Bmatrix} f_1(q_1) \\ f_2(q_2) \end{Bmatrix}=\begin{Bmatrix} F_{1m}+F_{1a}\sin(\Omega\tau) \\ F_{2m} \end{Bmatrix}, \tag{12}$$

$$[I]=\begin{bmatrix} 1 & 0 \\ 0 & 1 \end{bmatrix}, \qquad [\Xi]=2\begin{bmatrix} \zeta_{11}\omega_{11} & -\zeta_{12}\omega_{12} \\ -\zeta_{21}\omega_{21} & \zeta_{22}\omega_{22} \end{bmatrix}, \qquad [\Psi]=\begin{bmatrix} \omega_{11}^2 & -\omega_{12}^2 \\ -\omega_{21}^2 & \omega_{22}^2 \end{bmatrix}, \tag{13-15}$$

$$\zeta_{ii}=\frac{c_{ii}}{2m_{qi}\omega_{ii}}, \qquad \zeta_{12}=\frac{c_2}{2m_2\omega_{12}}, \qquad \zeta_{21}=\frac{c_1}{2m_2\omega_{21}}, \tag{16-18}$$

$$\omega_{ii}^2=\frac{k_i}{m_{qi}\omega_n^2}, \qquad \omega_{12}^2=\frac{k_2}{m_2\omega_n^2}, \qquad \omega_{21}^2=\frac{k_1}{m_2\omega_n^2}, \tag{19-21}$$

$$F_{1m}=\frac{\bar{F}_{1m}}{m_{q1}\omega_n^2 b_c}, \qquad F_{1a}=\frac{\bar{F}_{1a}}{m_{q1}\omega_n^2 b_c}, \qquad F_{2m}=\frac{\bar{F}_{2m}}{m_{q1}\omega_n^2 b_c}. \tag{22-24}$$

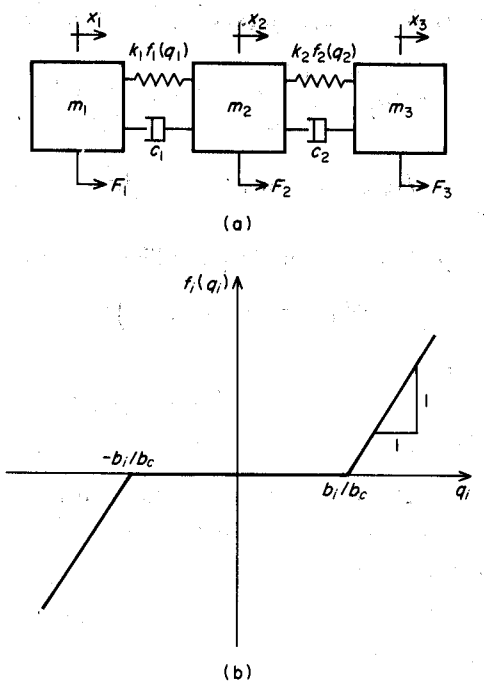

Figure 1. A non-linear three-degree-of-freedom semi-definite system: (a) physical model, $\bar{q}_1 = x_1 - x_2$, $\bar{q}_2 = x_2 - x_3$; (b) non-linear displacement function.

The non-linear displacement functions $f_i(q_i)$ for $i = 1$ and 2 are now chosen to describe the backlash or gap, which is equal to $2b_i$, as shown in Figure 1:

$$f_i(q_i) = \begin{cases} q_i + \dfrac{b_i}{b_c}, & q_i < -\dfrac{b_i}{b_c}, \\ 0, & -\dfrac{b_i}{b_c} \leqslant q_i \leqslant \dfrac{b_i}{b_c}, \\ q_i - \dfrac{b_i}{b_c}, & q_i > \dfrac{b_i}{b_c}. \end{cases} \tag{25}$$

The objectives of this study are: (i) to construct the approximate analytical solutions by using the harmonic balance method (HBM) and compare these with the results of digital and analog simulation; (ii) to study dynamic interactions between the system non-linearities for different cases and define spectral coupling issues; and (iii) to apply the proposed method to two practical cases.

3. SOLUTION METHODS

3.1. ANALYTICAL SOLUTION

To construct an approximate analytical solution using HBM, we assume that only $f_1(q_1)$ is non-linear as defined by equation (25), while $f_2(q_2) = q_2$. For the harmonic solution at the excitation frequency Ω only, letting $q_1 = q_{1m} + q_{1a} \sin(\Omega\tau + \phi_1)$, $q_2 = q_{2m} +$

$q_{2a}\sin(\Omega\tau+\phi_2)$, $f_1(q_1)=N_m q_{1m}+N_a q_{1a}\sin(\Omega\tau+\phi_1)$ and expressing [17]

$$N_m=\frac{1}{2\pi q_{1m}}\int_0^{2\pi} f(q_{1m}+q_{1a}\sin\varphi)\,\mathrm{d}\varphi, \tag{26}$$

$$N_a=\frac{1}{\pi q_{1a}}\int_0^{2\pi} f(q_{1m}+q_{1a}\sin\varphi)\sin(\varphi)\,\mathrm{d}\varphi, \qquad \varphi=\Omega\tau+\phi_1, \tag{27, 28}$$

we obtain the following equations by equating the like harmonics:

$$\begin{bmatrix} \omega_{11}^2 N_m & -\omega_{12}^2 \\ -\omega_{21}^2 N_m & \omega_{22}^2 \end{bmatrix}\begin{Bmatrix} q_{1m} \\ q_{2m} \end{Bmatrix}=\begin{Bmatrix} F_{1m} \\ F_{2m} \end{Bmatrix}, \tag{29}$$

$$\begin{bmatrix} (\omega_{11}^2 N_a-\Omega^2)+\mathrm{j}2\zeta_{11}\omega_{11}\Omega & -\omega_{12}^2-\mathrm{j}2\zeta_{12}\omega_{12}\Omega \\ \omega_{21}^2 N_a-\mathrm{j}2\zeta_{21}\omega_{21}\Omega & (\omega_{22}^2-\Omega^2)+\mathrm{j}2\zeta_{22}\omega_{22}\Omega \end{bmatrix}\begin{Bmatrix} q_{1a} \\ q_{2a} \end{Bmatrix}=\begin{Bmatrix} F_{1a} \\ 0 \end{Bmatrix}. \tag{30}$$

Equations (29) and (30) yield the following solutions in terms of non-linear algebraic equations for the mean and alternating components of the displacements:

$$q_{1m}=\frac{(F_{1m}\omega_{22}^2+F_{2m}\omega_{12}^2)}{N_m(\omega_{11}^2\omega_{22}^2-\omega_{12}^2\omega_{21}^2)}, \qquad q_{2m}=\frac{(F_{1m}\omega_{21}^2+F_{2m}\omega_{11}^2)}{(\omega_{11}^2\omega_{22}^2-\omega_{12}^2\omega_{21}^2)}, \tag{31, 32}$$

$$q_{1a}=\frac{F_{1a}\{(\omega_{22}^2-\Omega^2)^2+4\zeta_{22}^2\omega_{22}^2\Omega^2\}^{1/2}}{|\Lambda|}, \qquad q_{2a}=\frac{F_a\{(\Omega_{21}^2 N_a)^2+4\zeta_{21}^2\omega_{21}^2\Omega^2\}^{1/2}}{|\Lambda|}, \tag{33, 34}$$

$$\Lambda_r=(\omega_{11}^2 N_a-\Omega^2)(\omega_{22}^2-\Omega^2)-\omega_{21}^2\omega_{12}^2 N_a-4\zeta_{11}\zeta_{22}\omega_{11}\omega_{22}\Omega^2+4\zeta_{12}\zeta_{21}\omega_{12}\omega_{21}\Omega^2, \tag{35}$$

$$\Lambda_i=\Omega\{2\zeta_{11}\omega_{11}(\omega_{22}^2-\Omega^2)+2\zeta_{22}\omega_{22}(\omega_{11}^2 N_a-\Omega^2)-2\zeta_{12}\omega_{12}\omega_{21}^2 N_a-2\zeta_{21}\omega_{21}\omega_{12}^2\}, \tag{36}$$

$$\Lambda=\sqrt{\Lambda_r^2+\Lambda_i^2}. \tag{37}$$

The steady state frequency response can be obtained numerically by using the approximations for N_m and N_a developed earlier by Comparin and Singh [12]. The non-linearity can be regarded as an amplitude dependent stiffness. The non-linearity is hardening if the stiffness is increasing with q_{1a} and softening if it is decreasing with q_{1a}. The hardening or softening nature of the clearance non-linearity depends on the mean deflection q_{1m} and on whether the system is undergoing double- or single-sided vibro-impacts (the system is linear for the no-impact case), as shown in Figure 2. For the case of single-sided vibro-impacts, if the mean deflection q_{1m} is in the non zero stiffness stage; as q_{1a} increases the time spent in the backlash region increases, thereby reducing the average stiffness (softening effect). If, however, the mean deflection q_{1m} is within the backlash region, the average stiffness increases, as q_{1a} increases, for both double- and single-sided vibro-impacts, leading to a hardening effect. Furthermore, the modes of the two-degree-of-freedom system are dynamically coupled; hence the behavior of one mode will, in general, be influenced by the other. See references [12, 14] for further details.

3.2. DIGITAL AND ANALOG SIMULATIONS

A sixth order Runge–Kutta digital simulation method [18] is also used to solve equation (12) directly. Furthermore, an analog simulation is carried out on two COMDYNA GP-6 computers. The simulation circuit is shown in Figure 3. The backlash non-linearity of equation (25) is modeled by using a dead-space module (Model 9520). This simulation has been found to be difficult because the amplifiers become overloaded. Also the simulation is not very reliable at low frequencies due to signal drift. This problem has been resolved

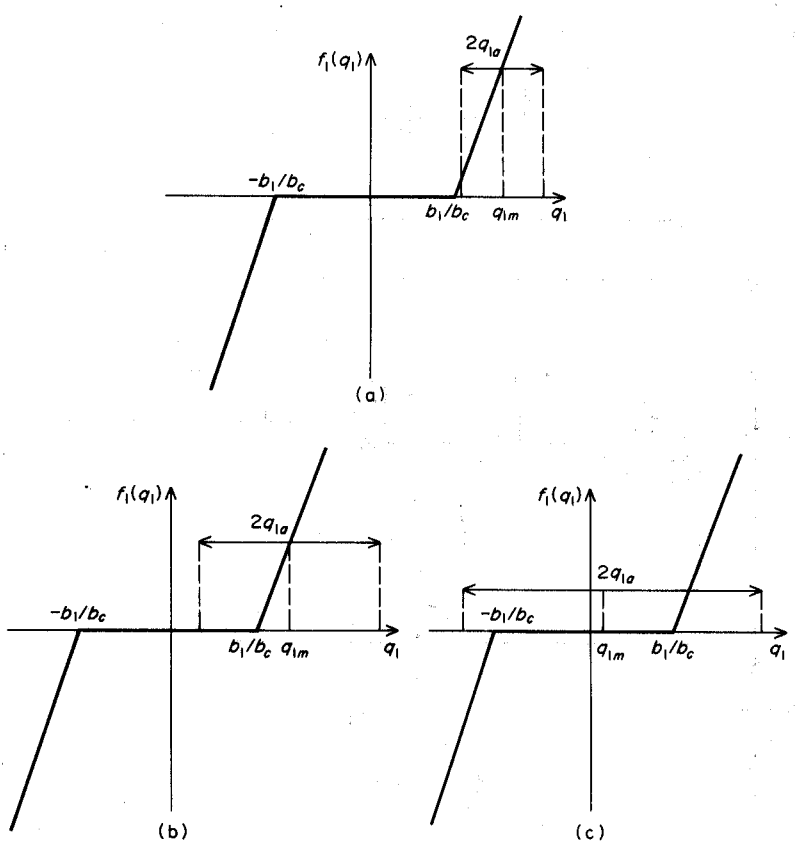

Figure 2. Different vibro-impact regimes: (a) no impact: (b) single-sided; (c) double-sided.

partially through time and magnitude scaling techniques. Still, as can be seen later, the quantitative match of analog response at low frequencies with other solution methods is not good. But, qualitative trends such as jump frequencies and non-harmonic solutions are predicted adequately.

3.3. TYPICAL SOLUTIONS

Frequency response results obtained by the methods discussed earlier are compared in Figures 4–6. Although there is good agreement between HBM and digital simulation, HBM obviously cannot predict quasi-periodic and chaotic solutions. Accordingly, digital simulation is used for such studies. The various types of solutions shown such as harmonic, non-harmonic (subharmonic, quasi-periodic and chaotic) were obtained by varying the initial conditions. Over certain frequency ranges the period 1 solution coexists with one or more higher period or non-periodic solutions. A period 2 and a period 64 subharmonic solution coexisting at a given frequency are shown in Figure 7. Typical numerical solutions are illustrated in Figures 8–10, which consist of time histories, phase-planes and Poincaré sections for different parameter values. Based on the simulations carried out, the following conclusions are drawn. First, subharmonics and non-periodic solutions dominate when the mean load F_{1m} is low. A smaller damping value ζ also predicts such motions. Secondly, a higher value ζ or F_{1m} leads to more period 1 solutions. Thirdly, two routes to chaos, namely the classical route of period doubling bifurcations and the quasi-periodic route

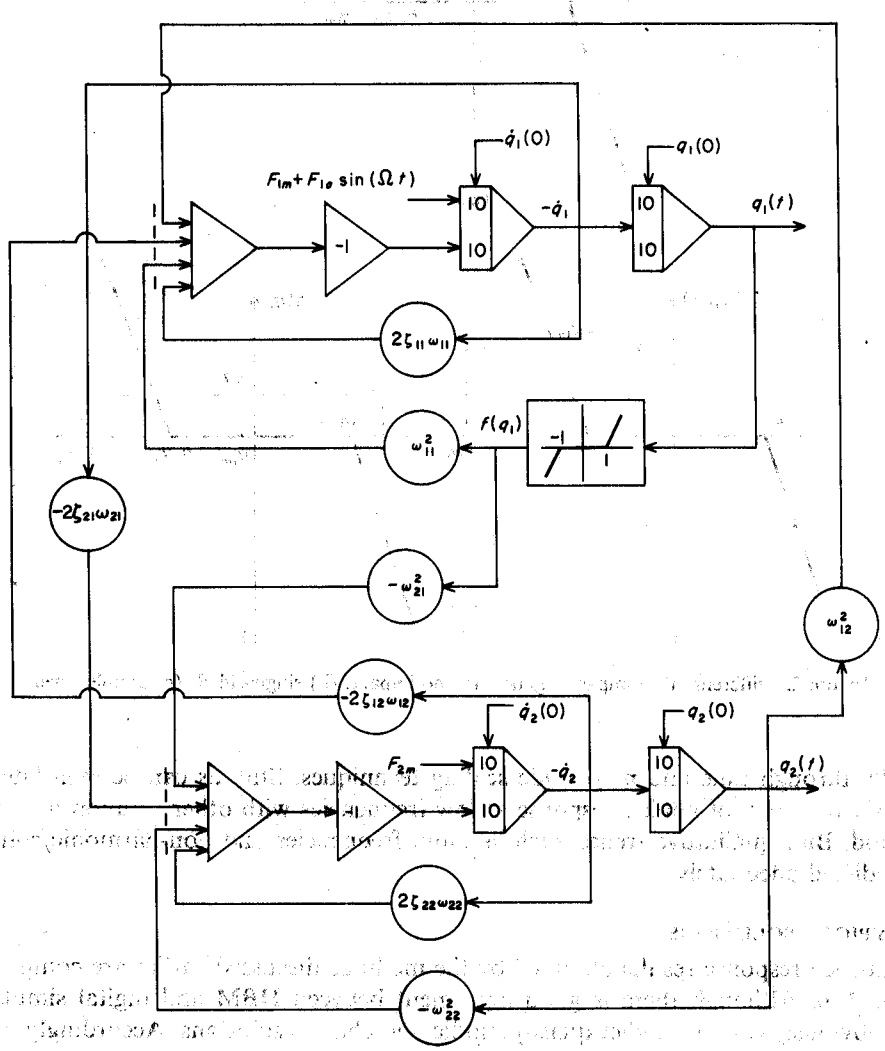

Figure 3. Analog simulation circuit for equation (2).

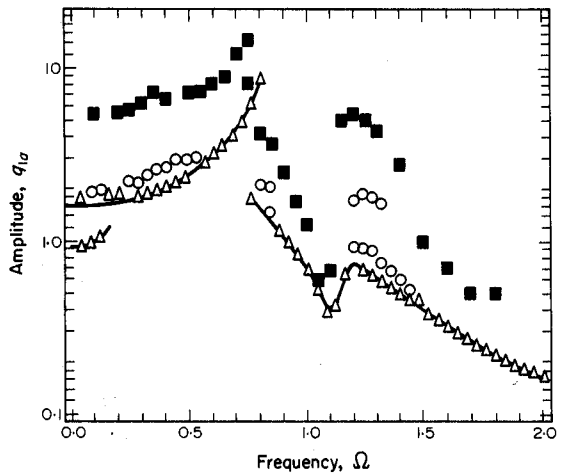

Figure 4. Frequency response of the non-linear system for $F_{1m}=F_{2m}=0{\cdot}25$, $F_{1a}=0{\cdot}50$, $\zeta_{11}=\zeta_{12}=\zeta_{21}=\zeta_{22}=0{\cdot}05$, $\omega_{11}=1{\cdot}0$, $\omega_{12}=\omega_{21}=0{\cdot}6$ and $\omega_{22}=1{\cdot}1$: ——, HBM; △, digital; ■, analog; ○, digital (non-harmonic).

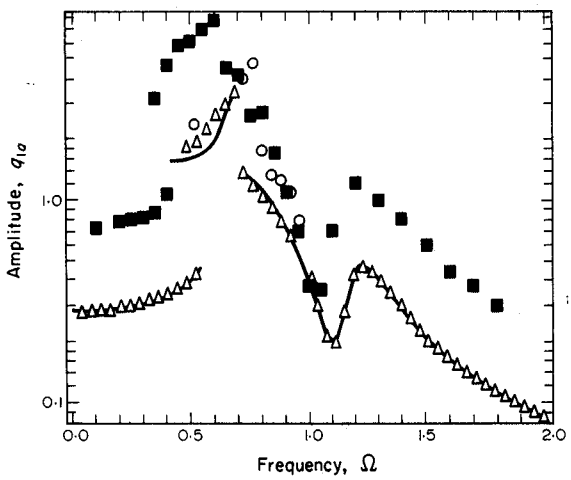

Figure 5. Frequency response of the non-linear system for $F_{1m}=F_{2m}=0{\cdot}25$, $F_{1a}=0{\cdot}25$, $\zeta_{11}=\zeta_{12}=\zeta_{21}=\zeta_{22}=0{\cdot}05$, $\omega_{11}=1{\cdot}0$, $\omega_{12}=\omega_{21}=0{\cdot}6$ and $\omega_{22}=1{\cdot}1$: ——, HBM; △, digital; ■, analog; ○, digital (non-harmonic).

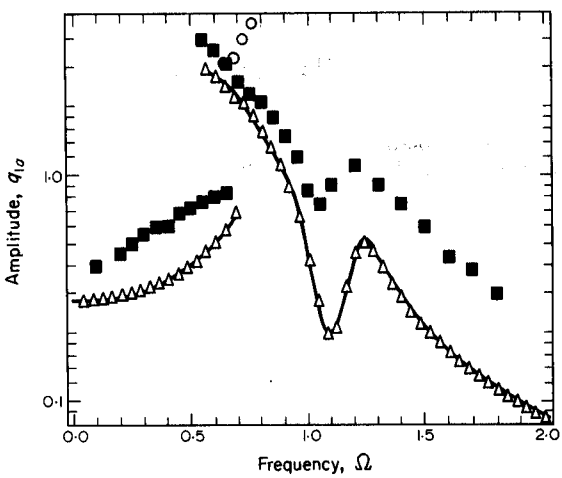

Figure 6. Frequency response of the non-linear system for $F_{1a}=F_{2m}=0{\cdot}25$, $F_{1m}=0{\cdot}50$, $\zeta_{11}=\zeta_{12}=\zeta_{21}=\zeta_{22}=0{\cdot}05$, $\omega_{11}=1{\cdot}0$, $\omega_{12}=\omega_{21}=0{\cdot}6$ and $\omega_{22}=1{\cdot}1$: ——, HBM; △, digital; ■, analog; ○, digital (non-harmonic).

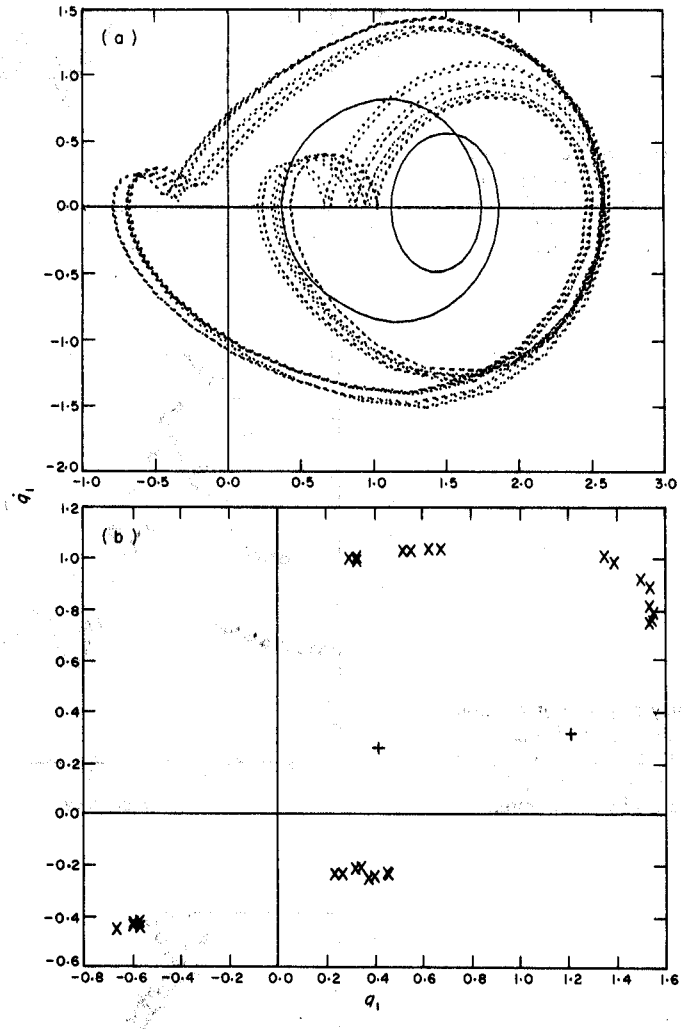

Figure 7. Co-existence of period 2 and period 64 subharmonic solutions: (a) phase-plane and (b) Poincaré section for $F_{1m}=F_{2m}=0{\cdot}25$, $F_{1a}=0{\cdot}5$, $\omega_{11}=1{\cdot}0$, $\omega_{12}=\omega_{21}=0{\cdot}6$ and $\omega_{22}=1{\cdot}1$, $\Omega=1{\cdot}32$.

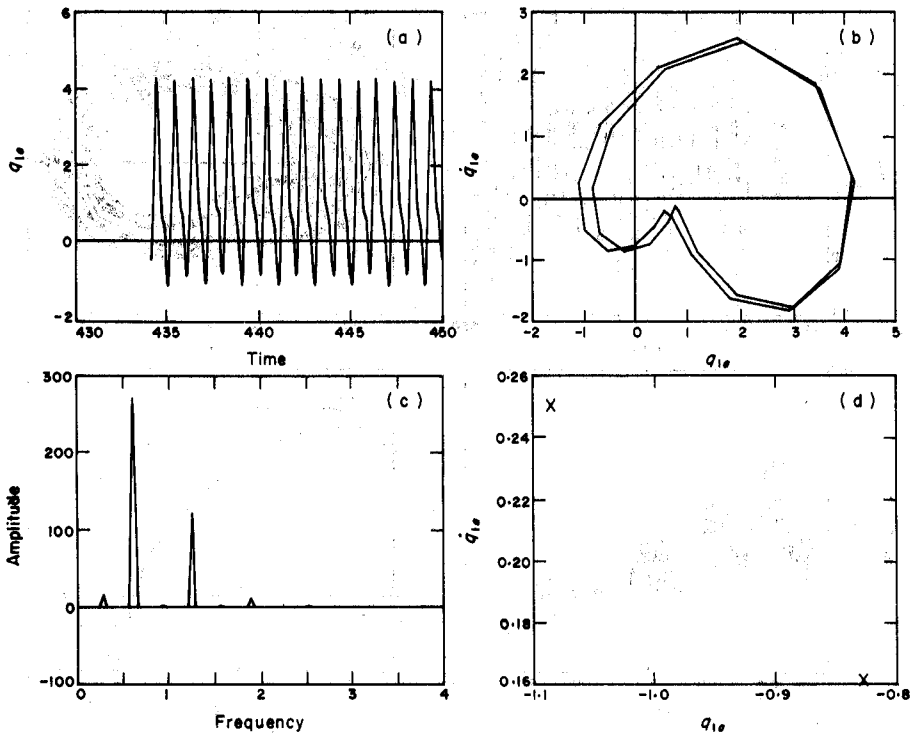

Figure 8. Subharmonic response: (a) time history, (b) phase-plane, (c) FFT and (d) Poincaré section for $F_{1m}=0{\cdot}25$, $F_{2m}=0{\cdot}50$, $F_{1a}=0{\cdot}25$, $\zeta=0{\cdot}05$, $\Omega=0{\cdot}62$, $\omega_{11}=1{\cdot}0$, $\omega_{12}=\omega_{21}=0{\cdot}8$ and $\omega_{22}=1{\cdot}1$.

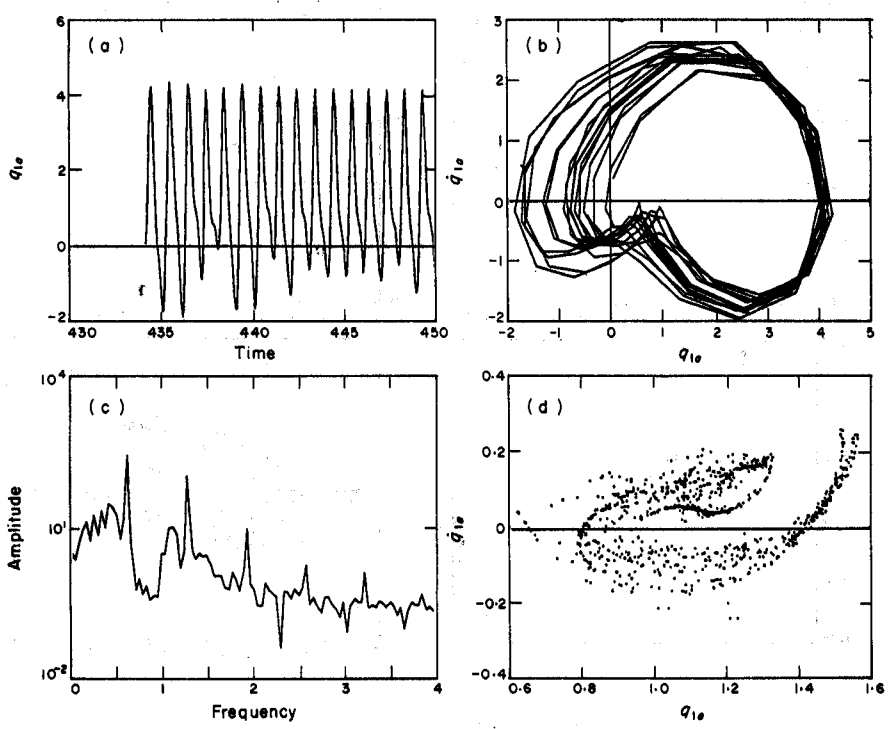

Figure 9. Chaotic response: (a) time history, (b) phase-plane, (c) FFT and (d) Poincaré section for $F_{1m}=0{\cdot}25$, $F_{2m}=0{\cdot}50$, $F_{1a}=0{\cdot}25$, $\zeta=0{\cdot}05$, $\Omega=0{\cdot}650$, $\omega_{11}=1{\cdot}0$, $\omega_{12}=\omega_{21}=0{\cdot}8$ and $\omega_{22}=1{\cdot}1$.

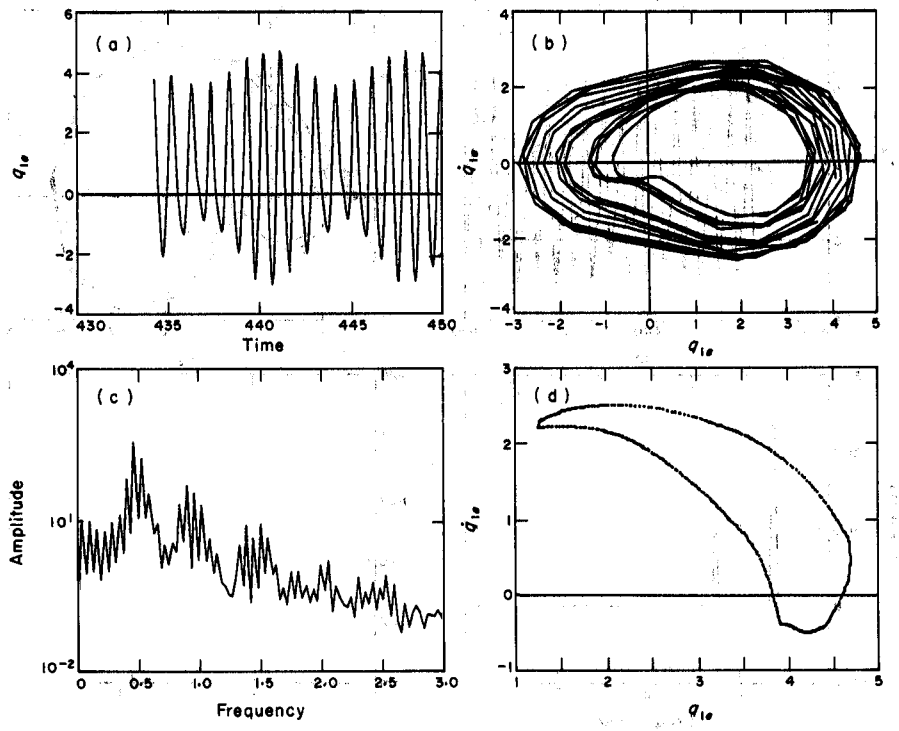

Figure 10. Quasi-periodic response: (a) time history, (b) phase-plane, (c) FFT and (d) Poincaré section for $F_{1m}=F_{2m}=F_{1a}=0{\cdot}25$, $\zeta=0{\cdot}03$, $\Omega=0{\cdot}48$, $\omega_{11}=1{\cdot}0$, $\omega_{12}=\omega_{21}=0{\cdot}6$ and $\omega_{22}=1{\cdot}1$.

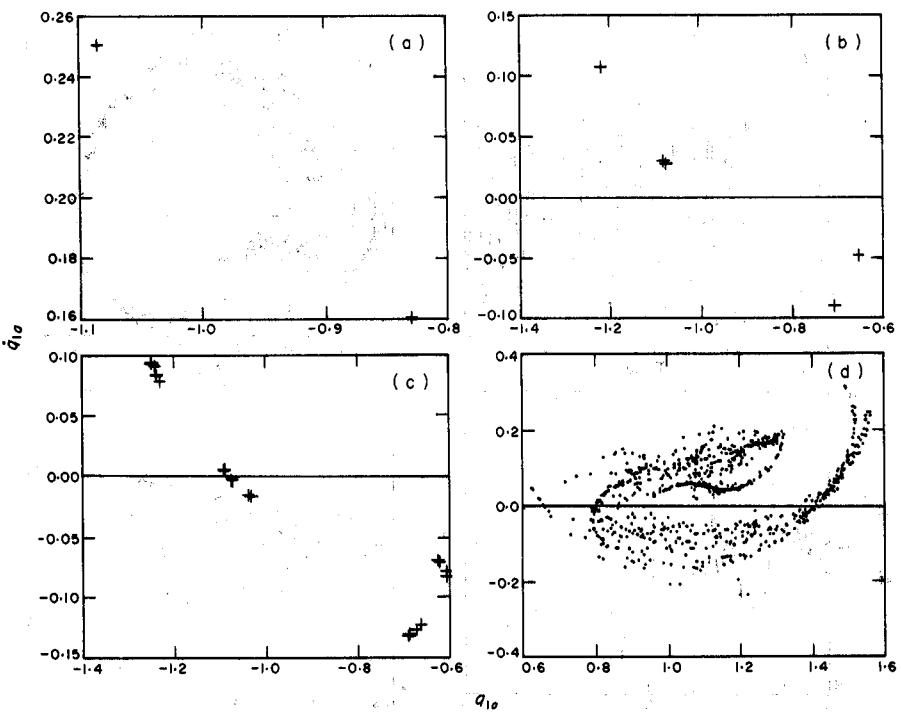

Figure 11. Poincaré sections showing the period doubling bifurcations to chaos for (a) $\Omega=0{\cdot}62$ (period 2), (b) $\Omega=0{\cdot}635$ (period 4), (c) $\Omega=0{\cdot}645$ (period 16) and (d) $\Omega=0{\cdot}650$ (chaotic): $F_{1m}=0{\cdot}25$, $F_{2m}=0{\cdot}5$, $F_{1a}=0{\cdot}25$, $\zeta=0{\cdot}05$, $\omega_{11}=1{\cdot}0$, $\omega_{12}=\omega_{21}=0{\cdot}8$ and $\omega_{22}=1{\cdot}1$.

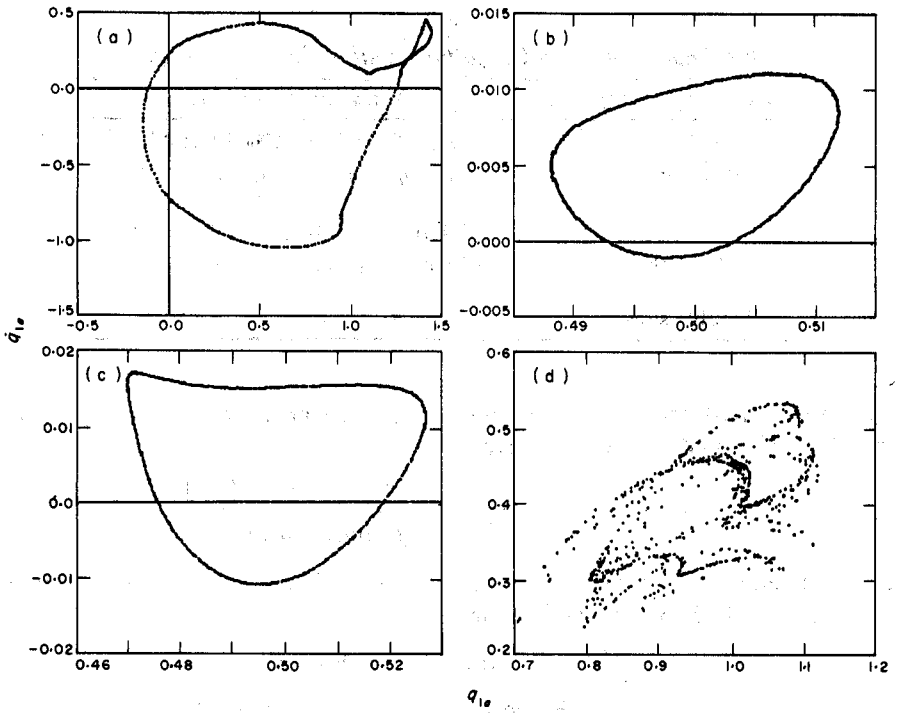

Figure 12. Poincaré sections showing the quasi-periodic route to chaos for (a) $\Omega = 0{\cdot}595$, (b) $\Omega = 0{\cdot}6$, (c) $\Omega = 0{\cdot}605$ and (d) $\Omega = 0{\cdot}61$: $\zeta = 0{\cdot}03$, $F_{1m} = F_{2m} = F_{1a} = 0{\cdot}25$, $\omega_{11} = 1{\cdot}0$, $\omega_{12} = \omega_{21} = 0{\cdot}6$ and $\omega_{22} = 1{\cdot}1$.

[13, 15, 19, 20], are seen in Figures 11 and 12. These observations are also compatible with the results reported by Kahraman and Singh [15] for a non-linear geared-rotor system. Most of the work reported here on chaotic motions has been qualitative, as the thrust of the paper is to study the spectral interactions.

4. SPECTRAL INTERACTIONS

As the MDOF non-linear system can show a wide range of dynamic behavior, general observations cannot be made without considering special cases. Also, a non-linear analysis can be complicated and expensive, so it is useful to know when a MDOF analysis is required and when a SDOF analysis is acceptable. Comparin and Singh [14] have proposed a qualitative scheme to classify dynamic interactions, while determining the frequency response of a non-linear MDOF system. The objective here is to use a similar scheme but examine various fundamental issues involved quantitatively. The formulation proposed here is along the lines of linear MDOF system theory, where the spectral (modal) coupling is influenced primarily by the damping ratio ζ and frequency spacing $\Delta\omega$ [21–23].

4.1. MATHEMATICAL FORMULATION

In order to facilitate the development, we construct an approximate analytical solution using HBM, and define transition frequencies $\Omega_{1,2}$ from the linear to the non-linear regime. Analytical conditions governing the vibro-impact regimes of Figure 2 are shown in Table 1; the terminology of recent publications on this topic [12–15] has been employed here.

TABLE 1

Vibro-impact types and conditions with reference to Figure 2

Vibro-impact type	Analytical conditions	
No impact	$\lvert q_{1m}-q_{1a}\rvert \geqslant 1,$	$\lvert q_{1m}+q_{1a}\rvert \geqslant 1$
	$q_{1m}+q_{1a} \leqslant 1,$	$q_{1m}-q_{1a} \geqslant -1$
Single-sided	$-1 \leqslant q_{1m}-q_{1a} \leqslant 1,$	$q_{1m}+q_{1a} \geqslant 1$
	$-1 \leqslant q_{1m}+q_{1a} \leqslant 1,$	$q_{1m}-q_{1a} \leqslant -1$
Double-sided	$q_{1m}-q_{1a} \leqslant -1,$	$q_{1m}+q_{1a} \geqslant 1$

It can be seen that one of the conditions for the transition is $q_{1m}-q_{1a}=1{\cdot}0$. From equations (31)–(37) and Table 1 we have

$$q_{1m}=1+\alpha, \qquad q_{1a}=\alpha=\frac{F_{1m}\omega_{22}^2+F_{2m}\omega_{12}^2}{(\omega_{11}^2\omega_{22}^2-\omega_{21}^2\omega_{12}^2)}. \tag{38, 39}$$

After considerable algebraic manipulations, we obtain the following polynomial equation in terms of Ω^2, which leads to $\Omega_{1,2}$:

$$\Omega^8+a_1\Omega^6+a_2\Omega^4+a_3\Omega^2+a_4=0, \tag{40}$$

$$a_1=4\zeta_{21}^2\omega_{21}^2-2\{\omega_{11}^2N_a+\omega_{22}^2-4\zeta_{21}\zeta_{12}\omega_{12}\omega_{21}\}, \tag{41}$$

$$a_2=2\{\omega_{11}^2\omega_{22}^2N_a-\omega_{12}^2\omega_{21}^2N_a\}+\{\omega_{11}^2N_a+\omega_{22}^2-4\zeta_{12}\zeta_{21}\omega_{12}\omega_{21}\}^2$$
$$+4\zeta_{21}\omega_{21}\{2\zeta_{21}\omega_{21}\omega_{12}^2+2\zeta_{12}\omega_{12}\omega_{21}^2N_a-2\zeta_{11}\omega_{11}\omega_{22}^2\}-\frac{F_{1a}^2}{\alpha^2}, \tag{42}$$

$$a_3=\{2\zeta_{21}\omega_{21}\omega_{12}^2+2\zeta_{21}\omega_{21}\omega_{12}^2N_a-2\zeta_{11}\omega_{11}\omega_{22}^2\}^2$$
$$-4\zeta_{21}\omega_{21}N_a\{\omega_{11}^2\omega_{22}^2-\omega_{12}^2\omega_{21}^2\}+2F_{1a}^2\omega_{22}^2(1-2\zeta_{22}^2)/\alpha^2, \tag{43}$$

$$a_4=N_a^2(\omega_{11}^2\omega_{22}^2-\omega_{12}^2\omega_{21}^2)-\frac{F_{1a}^2\omega_{22}^4}{\alpha^2}. \tag{44}$$

Here the coefficients depend on damping ratios, mean loads, alternating loads and the stiffness terms of equation (12). In order to examine the spectral interactions qualitatively, the following simpler equation is developed from equation (40) by neglecting damping terms:

$$\Omega^4+b_1\Omega^2+b_2=0, \tag{45}$$

$$b_1=\omega_{11}^2N_a+\omega_{22}^2-\frac{F_{1a}}{\alpha}, \qquad b_2=N_a(\omega_{11}^2\omega_{22}^2-\omega_{12}^2\omega_{21}^2)-\frac{F_{1a}}{\alpha}\omega_{22}^2. \tag{46, 47}$$

Three non-linear spectral interaction types can now be defined: (a) uncoupled resonances; (b) coupled but widely spaced resonances; and (c) coupled and closely spaced resonances.

4.2. UNCOUPLED RESONANCES

In this case the off-diagonal stiffness terms of $[\Psi]$ in equation (12) are much smaller than the diagonal terms. Approximating $\alpha=F_{1m}/\omega_{11}^2$ from equation (40) we obtain from equation (45) the transition frequencies as $\Omega_{1,2}=\omega_{11}\beta$ and ω_{22}, where

$\beta = (1 - F_{1a}/F_{1m})^{0.5}$. A jump transition occurs at the first resonance Ω_1. An immediate deviation from the linear system response can be noticed here, as the resonance frequencies depend on F_{1a}/F_{1m}. However, the governing equations are similar to the SDOF non-linear case. Hence, we can decompose such a two-degree-of-freedom system into two uncoupled SDOF systems, provided that there are no internal or combination resonances.

4.3. COUPLED BUT WIDELY SPACED RESONANCES

Here the coupling terms in equation (12) are not negligible, but the resonances are widely spaced. The simplified formulation for $\Omega_{1,2}$ given by equation (45) shows that the system behaves in a non-linear manner in the vicinity of the jump Ω_1, and in a linear manner around the second resonance at Ω_2. The addition of damping modifies this, as will be shown later.

4.4. CLOSELY COUPLED RESONANCES

This case is investigated using equation (40) with four key parameters, which are damping ratio, mean loads, alternating load and frequency spacing $\Delta\omega$. First, we examine the effect of damping ratio ζ in Figures 13 and 14 (for $F_{1m}=0{\cdot}5$, $F_{2m}=0{\cdot}25$, $F_{1a}=0{\cdot}25$, $\omega_{11}=1{\cdot}0$, $\omega_{12}=\omega_{21}=0{\cdot}6$ and $\omega_{22}=1{\cdot}1$); for simplicity in analysis, we assume that $\zeta_{11}=\zeta_{12}=\zeta_{21}=\zeta_{22}=\zeta$. By decreasing ζ, the non-linear regime of the first mode increases, thereby interacting strongly with the other resonance. It can be seen that if the linear natural

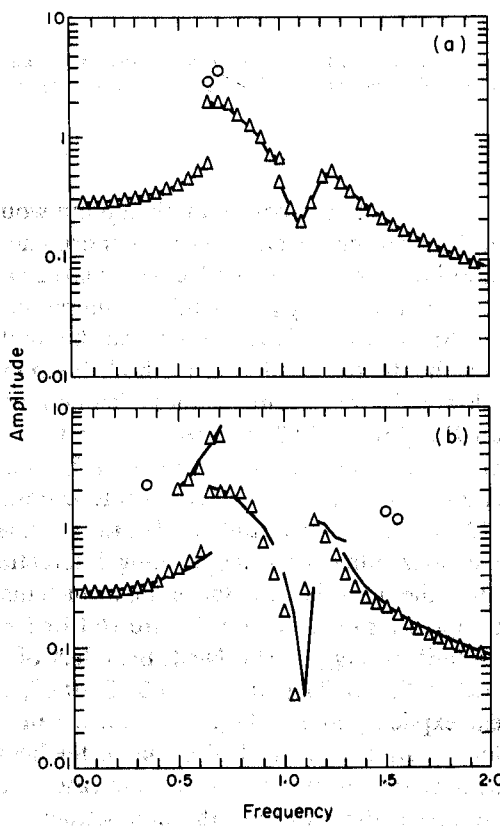

Figure 13. Effect of ζ on the non-linear interactions in the q_{1a} spectrum for (a) $\zeta=0{\cdot}05$ and (b) $\zeta=0{\cdot}02$: ——, HBM; △, digital; ○, digital (non-harmonic).

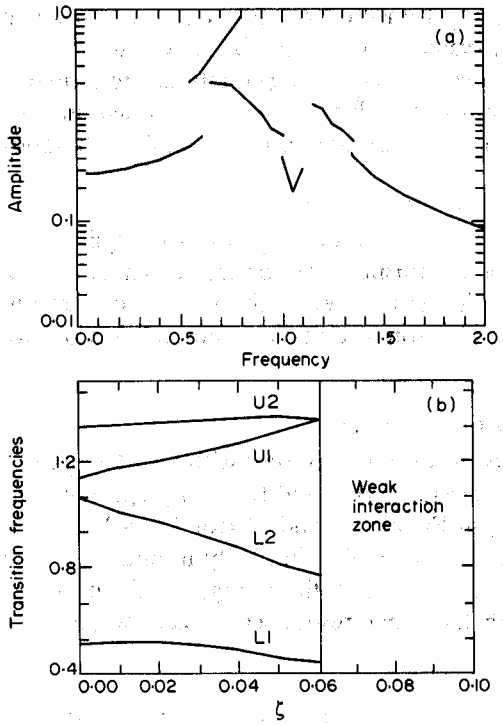

Figure 14. Effect of ζ on the interactions in the q_{1a} spectrum for (a) $\zeta = 0{\cdot}0$ and (b) transition frequencies, where L1 and L2 are lower transition frequencies, and U1 and U2 are upper transition frequencies: ——, HBM; △, digital.

frequencies ($\omega_{n1} = 0{\cdot}86$ and $\omega_{n2} = 1{\cdot}2$) are close enough, a jump would occur at the second resonance. An increase in ζ causes the system to become more linear, with a reduction in the spectral range of the non-linear regime. This effect is in marked contrast with the linear system behavior, where an increase in ζ leads to stronger interactions, especially when the modes are closely coupled. Most of these observations can be made from equation (40). However, when we employ the digital simulation method, the number of non-harmonic solutions increases as we lower ζ. Hence some of these distinctions become less obvious.

The effect of mean load F_{1m} (for $\zeta = 0{\cdot}03$, $F_{2m} = 0{\cdot}25$, $F_{1a} = 0{\cdot}25$, $\omega_{11} = 1{\cdot}0$, $\omega_{12} = \omega_{21} = 0{\cdot}6$ and $\omega_{22} = 1{\cdot}1$) is illustrated in Figure 15. An increase in F_{1m} tends to make the system more linear, and a lower F_{1m} causes stronger spectral interactions. Since there are two mean loads in equation (12), a comparative study of F_{1m} *vs.* F_{2m} has also been conducted. It seems that F_{1m} has a greater influence in controlling interactions than F_{2m}. This is because F_{1m} is associated with the sinusoidal excitation F_{1a}, which makes the first resonance dominant over the second one, as is evident from Figure 16 (for $\zeta = 0{\cdot}03$, $F_{1m} = 0{\cdot}5$, $F_{1a} = 0{\cdot}25$, $\omega_{11} = 1{\cdot}0$, $\omega_{12} = \omega_{21} = 0{\cdot}65$ and $\omega_{22} = 1{\cdot}1$). Next, the effect of frequency spacing $\Delta\omega$ on interactions is examined in Figure 17 (for $F_{1m} = 0{\cdot}3$, $\zeta = 0{\cdot}03$, $F_{2m} = 0{\cdot}25$, $F_{1a} = 0{\cdot}25$). This term does not appear explicitly in equation (40), but it can be varied by adjusting the stiffness terms of $[\Psi]$ in equation (12) which also change the linear natural frequencies. It is seen that, as in a linear system, a decrease in $\Delta\omega$ increases the interactions, and the farther the frequencies are apart, the lesser are the interactions. Finally, the alternating load F_{1a}, as seen in Figures 18 and 19 (for $\zeta = 0{\cdot}03$, $F_{2m} = 0{\cdot}25$, $F_{1m} = 0{\cdot}5$, $\omega_{11} = 1{\cdot}0$, $\omega_{12} = \omega_{21} = 0{\cdot}6$ and $\omega_{22} = 1{\cdot}1$), has a dramatic effect on the response. If $F_{1a} > F_{1m}$, then the non-

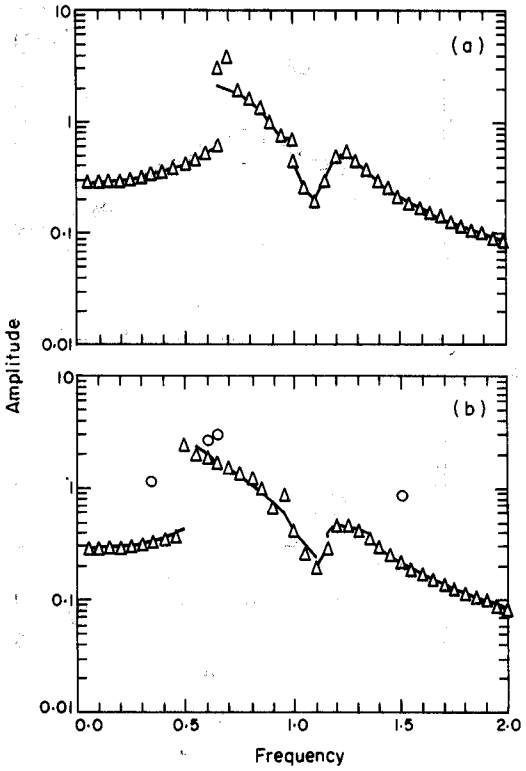

Figure 15. Effect of F_{1m} on the interactions in the q_{1a} spectrum for (a) $F_{1m}=0{\cdot}50$ and (b) $F_{1m}=0{\cdot}25$: ——, HBM; △, digital; ○, digital (non-harmonic).

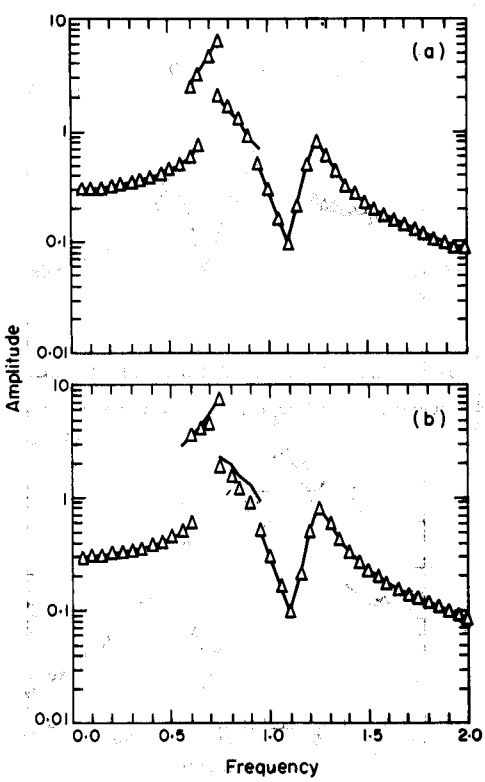

Figure 16. Effect of F_{2m} on the interactions in the q_{1a} spectrum for (a) $F_{2m}=0{\cdot}50$ and (b) $F_{2m}=0{\cdot}3$: ——, HBM; △, digital.

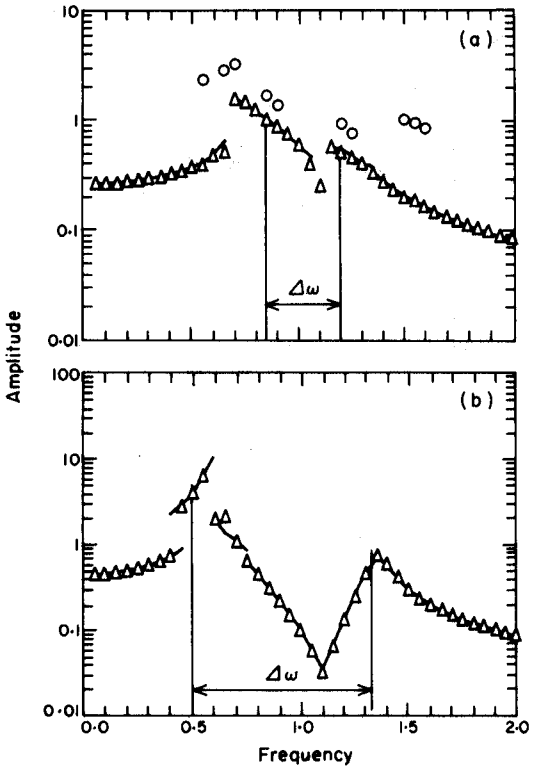

Figure 17. Effect of $\Delta\omega$ on the non-linear interactions in the q_{1a} spectrum for: (a) $\omega_{11}=1{\cdot}0$, $\omega_{12}=\omega_{21}=0{\cdot}6$ and $\omega_{22}=1{\cdot}1$; (b) $\omega_{12}=\omega_{21}=0{\cdot}82$. ——, HBM; △, digital; ○, digital (non-harmonic).

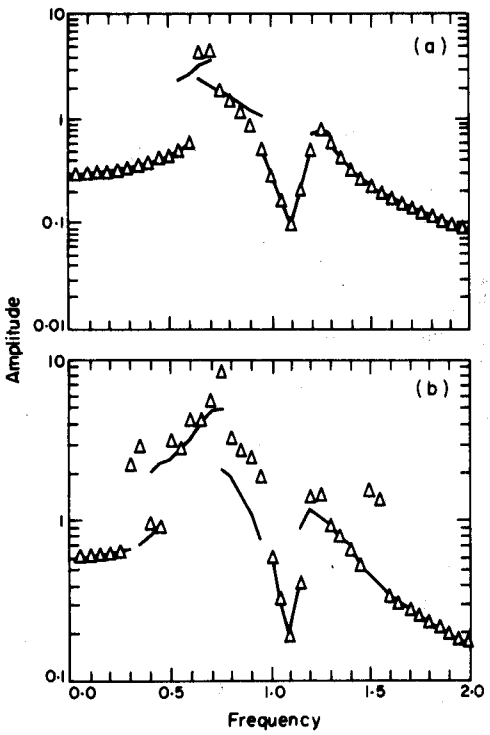

Figure 18. Effect of F_{1a} on the non-linear interaction in the q_{1a} spectrum for (a) $F_{1a}=0{\cdot}25$ and (b) $F_{1a}=0{\cdot}5$: ——, HBM; △, digital.

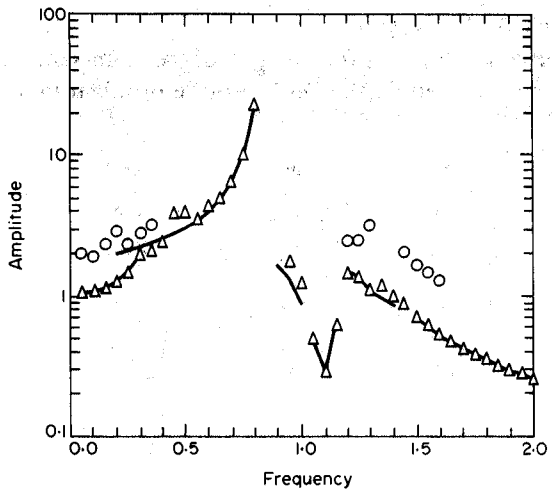

Figure 19. Effect of F_{1a} on the non-linear interactions in the q_{1a} spectrum for $F_{1a}=0{\cdot}75$: ——, HBM; △, digital; ○, digital (non-harmonic).

linear regimes start right from $\Omega=0$, and a highly non-linear system is seen for higher F_{1a}. A lower F_{1a} reduces the interaction between the resonances.

The following quantitative relationship has been developed, through a curve fit of the simulated data given in Figures 13–19. Spectral interactions are weak when

$$\Delta\omega \geqslant \delta, \qquad \delta = 0{\cdot}25 \exp(-\hat{F}_1)\hat{F}_2^{0{\cdot}15}\zeta^{-0{\cdot}5}, \tag{48}$$

where $\hat{F}_1 = F_{1a}/F_{1m}$ and $\hat{F}_2 = F_{1a}/F_{2m}$. This relationship is only valid when $\hat{F}_1 \leqslant 1{\cdot}0$, $\hat{F}_2 \leqslant 1{\cdot}0$ and $F_{1a} \leqslant 0{\cdot}5$. When these conditions are not met, it is not easy to curve fit due to qualitative changes in the frequency response. Also equation (48) corresponds to the linear response at $\Omega=0$.

4.5. EFFECT OF INTERACTIONS ON ANALOG SIMULATION

The results of analog computer simulation are compared with solutions yielded by HBM and digital simulation in Figures 4–6. Figures 4 and 5 correspond to $F_{1a}=0{\cdot}50$ and $0{\cdot}25$, respectively. Increasing F_{1a} introduces more discrepancies between the response predicted by the analog computer and the response predicted by the other two solution methods. When equation (48) is used to check the interactions in Figure 4 we find that $\Delta\omega/\delta > 1$. This implies that the interactions are not strong, as can be seen in the results. But, equation (48) cannot be used for Figure 4 as $\hat{F}_1 > 1$. In Figure 6, with $F_{1m}=0{\cdot}50$ and $F_{1a}=0{\cdot}25$, the discrepancy between the analog simulation results and the results by the other two methods is smaller than the previous two cases. Although there is no quantitative match, it can be seen that there is a definite reduction in the discrepancy when the interactions are weak. Also, for this case, $\Delta\omega/\delta > 1$, which indicates that the interactions are weak, as confirmed by the results. An improved technique is obviously needed if systems with strong interactions are to be studied with an analog computer.

5. PRACTICAL EXAMPLE CASES

The following two practical cases are considered to check some of the observations made earlier: (a) an automotive transmission rattle problem [10]; and (b) Munro's experiment on a spur gear pair [24].

5.1. AUTOMOTIVE NEUTRAL RATTLE

Singh *et al.* [10] have developed a four-degree-of-freedom semi-definite model (shown schematically in Figure 20) to study the neutral rattle problem in a manual transmission.

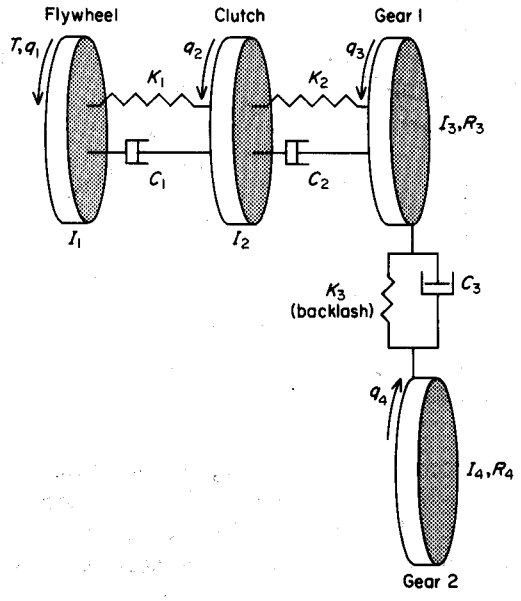

Figure 20. The four-degree-of-freedom torsional model of transmission for neutral rattle study with viscous damping: $K_1 = 50$ Nm/rad, $K_2 = 1{\cdot}44 \times 10^4$ Nm/rad, $K_3 = 2{\cdot}22 \times 10^8$ N/m, $I_1 = 0{\cdot}16$ kg m^2, $I_2 = 3{\cdot}35 \times 10^{-3}$ kg m^2, $I_3 = 1{\cdot}53 \times 10^{-3}$ kg m^2, $I_4 = 3{\cdot}68 \times 10^{-3}$ kg m^2.

A linear analysis of the system has been carried out and the corresponding eigensolutions are shown in Table 2. From these results it is obvious that $q_2 \approx q_3$ over the frequency range of interest. Hence this physical system can be reduced to a three-degree-of-freedom semi-definite non-linear model by lumping q_2 and q_3 together, and by defining clearance type non-linearities in the clutch and at the gear mesh. We now apply the formulation developed earlier. As the linear natural frequencies of the reduced system are far apart ($\omega_3/\omega_2 = 33{\cdot}32$), we can expect weak spectral interactions between the resonances.

TABLE 2

Modal data for the automotive system of Figure 20

Modal index	Natural frequency (rad/s)	Modal displacements (rad)			
		q_1	q_2	q_3	$(R_4/R_3)q_4$
1	0·0	1·0	1·0	1·0	1·0
2	84·13	−0·046	0·998	1·0	1·0
3	2 805·47	$-4{\cdot}0 \times 10^{-5}$	1·0	−0·828	−0·846
4	19 856·0	$-1{\cdot}76 \times 10^{-5}$	$2{\cdot}2 \times 10^{-3}$	−0·200	2·0833

Results for this system with only one non-linearity are presented in Figure 21. It is seen that the system is indeed weakly coupled and that various parameters do not promote dynamic interactions strongly. Equation (48) gives $\Delta\omega/\delta \gg 1$, which confirms that the interactions are indeed weak. However, this system has shown other interesting character-

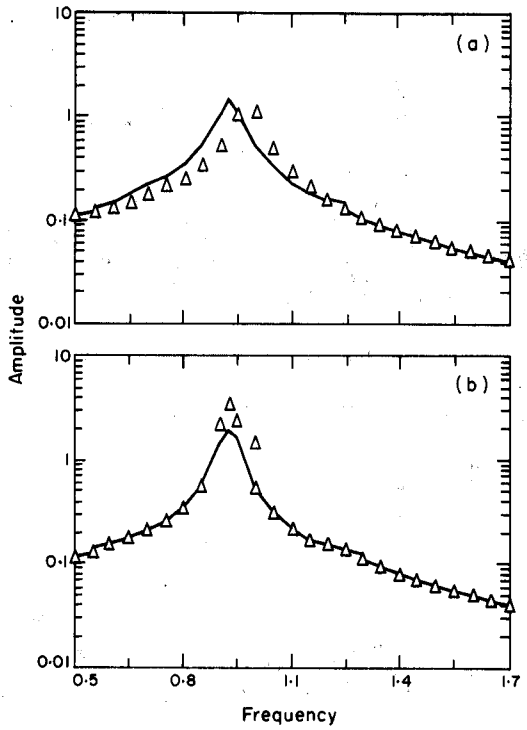

Figure 21. Frequency response q_{1a} of the neutral gear rattle model: ——, HBM; △, digital; (a) $C_3 = 0{\cdot}75$ Ns/m, (b) $C_3 = 0{\cdot}25$ Ns/m.

istics. For instance, when the non-linearity is only in the clutch, the higher period or chaotic solutions are few and difficult to observe. Conversely, the gear backlash tends to increase such solutions over a wide range of parameters.

5.2. MUNRO'S EXPERIMENT ON A SPUR GEAR PAIR [24]

The solutions of section 4.1 are now compared with the experimental results of Munro [24], who measured the dynamic response of a spur gear pair. Kahraman and Singh [15] have developed the following two-degree-of-freedom model to simulate this experiment:

$$\begin{bmatrix} 1 & 0 \\ 1 & 1 \end{bmatrix} \begin{Bmatrix} \ddot{q}_1(t) \\ \ddot{q}_2(t) \end{Bmatrix} + 2 \begin{bmatrix} \zeta_{11} & \zeta_{12} \\ 0 & \zeta_{22} \end{bmatrix} \begin{Bmatrix} \dot{q}_1(t) \\ \dot{q}_2(t) \end{Bmatrix} + \begin{bmatrix} \kappa_{11} & \kappa_{12} \\ 0 & 1 \end{bmatrix} \begin{Bmatrix} q_1(t) \\ f_2(q_2(t)) \end{Bmatrix}$$

$$= \begin{Bmatrix} 0 \\ F_m + F_a \Omega^2 \sin(\Omega t) \end{Bmatrix}. \tag{49}$$

Here q_{1a} corresponds to the bearing displacement and q_{2a} to the dynamic transmission error, and $f_2(q_2)$ is the backlash function given by equation (25). Due to the change in the nature of the sinusoidal excitation, from the external F_{1a} to the internal static transmission error given by $F_a\Omega^2$, equations (40)–(44) are modified as follows:

$$b_0\Omega^8 + b_1\Omega^6 + b_2\Omega^4 + b_3\Omega^2 + b_4 = 0, \tag{50}$$

$$b_0 = -F_a^2/\alpha^2, \qquad b_1 = a_1 + 2F_a^2\kappa_{22}(1 - 2\zeta_{22}^2)/\alpha^2, \tag{51, 52}$$

$$b_2 = a_2 - F_a^2\kappa_{22}^2/\alpha^2, \qquad b_3 = a_3 - 2F_a^2\kappa_{22}(1 - 2\zeta_{22}^2)/\alpha^2, \tag{53, 54}$$

$$b_4 = a_4 + F_a^2\kappa_{22}^2/\alpha^2, \qquad \kappa_{22} = \omega_{22}^2. \tag{55, 56}$$

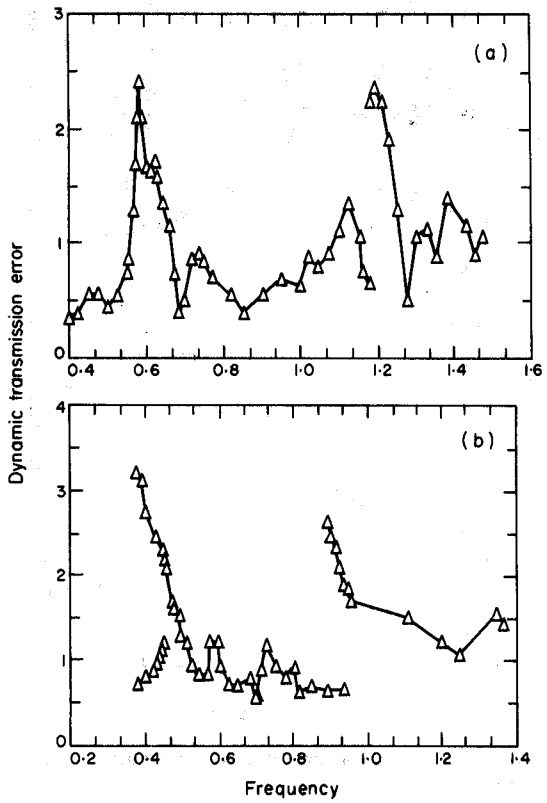

Figure 22. Measured data of Munro's experiment [24] on a spur gear pair for (a) 1/4 of the design load and (b) 3/4 of the design load.

These equations are used to study the spectral interactions for the following sets of numerical parameters: (i) $F_m = 0{\cdot}0579$, $F_a = 0{\cdot}0393$, $\hat{F} = F_a/F_m = 0{\cdot}6788$, $\zeta_{11} = 0{\cdot}01$, $\zeta_{12} = 0{\cdot}00375$, $\zeta_{22} = 0{\cdot}015$, $\kappa_{11} = 1{\cdot}007$, $\kappa_{12} = 0{\cdot}4919$ (1/4 of the design load); and (ii) $F_m = 0{\cdot}146$, $F_a = 0{\cdot}0178$, $\hat{F} = 0{\cdot}122$, $\kappa_{11} = 0{\cdot}9660$ (3/4 of the design load). According to equation (50), we expect stronger interactions for the first case since $\hat{F}$ is much higher. This is confirmed in Figure 22, where the measured spectra for the two cases are given. The jump frequencies ($\Omega_2 = 1{\cdot}26$ for 3/4 design load and $\Omega_1 = 0{\cdot}52$, $\Omega_2 = 0{\cdot}89$ for 1/4 design load) predicted by equation (50) match very well the measured data. As the excitation amplitude is $F_a\Omega^2$, the system has a linear response at lower frequencies and a non-linear response at higher frequencies. This behaviour reduces the possibility of very strong non-linear interactions, as seen in Figure 22. Hence, the above system can be classified as one with moderate spectral coupling. Application of equation (48) to this system confirms the nature of the coupling.

6. CONCLUDING REMARKS

In this study HBM is used to develop a scheme to classify dynamic interactions between resonances in a non-linear MDOF system. However, as seen in the digital solutions, the number of non-harmonic solutions increases as such interactions become stronger. This obviously reduces the effectiveness of HBM to quantify spectral interactions. However, the qualitative nature of the response can still be predicted. Also, with an increase in

interactions, analog simulations begin to deviate from digital and HBM solutions. Accordingly, our future work will focus on resolving these issues. The emphasis will be on practical transmission and suspension systems with multiple clearances.

ACKNOWLEDGMENTS

We wish to acknowledge the Transportation Research Endowment Program (Honda) at The Ohio State University for supporting this research. We thank C. Lee for his help in the analog simulation studies.

REFERENCES

1. C. N. BAPAT, N. POPPLEWELL and K. MACLACHLAN 1983 *Journal of Sound and Vibration* **87**, 19–40. Stable periodic motions of an impact pair.
2. G. S. WHISTON 1979 *Journal of Sound and Vibration* **67**, 179–186. Impacting under harmonic excitation.
3. S. DUBOWSKY and F. FREUDENSTEIN 1971 *ASME Journal of Engineering for Industry* **93**, 310–316. Dynamic analysis of mechanical systems with clearances, part 2: dynamic response.
4. W. S. LOUD 1968 *International Journal of Non-linear Mechanics* **3**, 273–293. Branching phenomena for periodic solutions of non-autonomous piecewise linear systems.
5. S. NATSIAVAS 1989 *Journal of Sound and Vibration* **134**, 315–331. Periodic response and stability of oscillators with symmetric trilinear restoring force.
6. S. W. SHAW and J. SHAW 1989 *American Society of Mechanical Engineers, Journal of Applied Mechanics* **56**, 168–174. The onset of chaos in a two-degree-of-freedom impacting system.
7. Y. STEPANENKO and T. S. SANKAR 1986 *American Society of Mechanical Engineers, Journal of Dynamic Systems, Measurement and Control* **108**, 9–16. Vibro-impact analysis of control systems with mechanical clearances and its application to robotic actuators.
8. M. A. VELUSWAMI, F. R. E. CROSSLEY and G. HORVAY 1975 *American Society of Mechanical Engineers, Journal of Engineering for Industry* **97**, 828–835. Multiple impacts of a ball between two plates, part 2: mathematical modeling.
9. G. R. TOMLINSON and J. LAM 1984 *Journal of Sound and Vibration* **96**, 111–125. Frequency response characteristics of structures with single and multiple clearance type non-linearities.
10. R. SINGH, H. XIE and R. J. COMPARIN 1989 *Journal of Sound and Vibration* **131**, 177–196. Analysis of automotive neutral gear rattle.
11. M. A. VELUSWAMI and F. R. E. CROSSLEY 1975 *American Society of Mechanical Engineers, Journal of Engineering for Industry* **97**, 820–827. Multiple impacts of a ball between two plates, part 1: some experimental observations.
12. R. J. COMPARIN and R. SINGH 1989 *Journal of Sound and Vibration* **134**, 259–290. Frequency response characteristic of an impact pair.
13. A. KAHRAMAN and R. SINGH 1990 *Journal of Sound and Vibration* **142**, 49–75. Nonlinear dynamics of a spur gear pair.
14. R. J. COMPARIN and R. SINGH 1990 *Journal of Sound and Vibration* **142**, 101–124. Frequency response of multi-degree-of-freedom systems with clearances.
15. A. KAHRAMAN and R. SINGH 1990 *Journal of Sound and Vibration* **144**, 469–506. Nonlinear dynamics of a geared rotor–bearing system with multiple clearances.
16. A. G. HADDOW, A. D. S. BARR and D. T. MOOK 1984 *Journal of Sound and Vibration* **97**, 451–473. Theoretical and experimental study of modal interaction in a two-degree-of-freedom structure.
17. A. GELB and W. E. VAN DER WELDE 1968 *Multiple Input Describing Functions and Nonlinear System Design*. New York: McGraw-Hill.
18. IMSL INC. 1986 IMSL User's Manual.
19. F. C. MOON 1987 *Chaotic Vibrations*. New York: John Wiley.
20. J. M. T. THOMSON and H. B. STEWART 1986 *Nonlinear Dynamics and Chaos*. Chichester: John Wiley.
21. R. J. ALLEMANG, D. L. BROWN, R. ZIMMERMAN and M. MERGEAY 1979 SAE Paper No. 790221. Parameter estimation techniques for modal analysis.

22. D. E. NEWLAND 1987 *Journal of Sound and Vibration* **112**, 69–96. On the modal analysis of nonconservative systems.
23. R. E. D. BISHOP, G. M. L. GLADWELL and S. MICHAELSON 1965 *The Matrix Analysis of Vibration*. Cambridge University Press.
24. R. G. MUNRO 1962 *Ph.D. Dissertation, University of Cambridge*. The dynamic behavior of spur gears.